

# Combined Machine Learning and CALPHAD Approach for Discovering Processing-Structure Relationships in Soft Magnetic Alloys\*

Rajesh Jha,<sup>1,†</sup> Nirupam Chakraborti,<sup>2</sup> David R. Diercks,<sup>3</sup> Aaron P. Stebner,<sup>1</sup> and Cristian V. Ciobanu<sup>1,‡</sup>

<sup>1</sup>*Department of Mechanical Engineering, Colorado School of Mines, Golden, Colorado 80401, USA*

<sup>2</sup>*Department of Metallurgical and Materials Engineering,  
Indian Institute of Technology Kharagpur, West Bengal, India*

<sup>3</sup>*Department of Metallurgical and Materials Engineering,  
Colorado School of Mines, Golden, Colorado 80401, USA*

(Dated: June 1, 2022)

FINEMET is a class of alloys which have superior soft magnetic properties due to the presence of Fe<sub>3</sub>Si nanocrystals with a specific size and nanocrystalline volume fraction. With the purpose to guide future design of these alloys, we aim to investigate relationships between select processing parameters or inputs (composition, temperature, annealing time) and two structural parameters, specifically, the mean radius and volume fraction of the Fe<sub>3</sub>Si nanocrystals. To this end, we have devised a combined CALPHAD and machine learning approach that led to well-calibrated meta-models able to predict structural parameters quickly and accurately for any desired inputs. In order to generate data for the mean radius and volume fraction of Fe<sub>3</sub>Si nanocrystals, we have used a precipitation model based in the software Thermocalc to perform annealing simulations at a set of temperatures (490–550 °C) and for varying Fe and Si concentrations (Fe<sub>72.89+x</sub>Si<sub>16.21-x</sub>B<sub>6.90</sub>Nb<sub>3</sub>Cu<sub>1</sub>,  $-3 \leq x \leq 3$  atomic %). Thereafter, we used the data to develop metamodels for the mean radius and volume fraction via the  $k$ -Nearest Neighbour algorithm. The metamodels are shown to reproduce closely the trends obtained from the precipitation model over the entire annealing timescale. Our further analysis via parallel coordinate charts shows the effect of composition, temperature, and annealing time, and helps identify combinations thereof that lead to the desired mean radius and volume fraction for the nanocrystalline phase. This approach utilizes experimental (thermodynamic and kinetic) databases from the CALPHAD approach so as to capture the physics of nucleation and growth, while the machine learning algorithm provides the robustness needed to analyze the effects of processing parameters for this complex precipitation problem. This work contributes to understanding the linkages between processing parameters and desired microstructural characteristics (crystal size and volume fraction) responsible for achieving targeted properties, and illustrates ways to reduce the time from alloy discovery to deployment.

## I. INTRODUCTION

FINEMET alloys belong to a class of soft magnetic alloys based on the Fe-Si-Nb-B-Cu system.<sup>1</sup> In comparison with other soft magnets, FINEMET alloys possess high saturation magnetization<sup>1,2</sup> and high permeability,<sup>2-6</sup> low core loss,<sup>1-4,6</sup> low magnetostriction,<sup>1-4,6,7</sup> excellent temperature characteristics,<sup>2</sup> small aging effects,<sup>2</sup> and excellent high frequency characteristics.<sup>1-4,6</sup> As a result, FINEMET alloys have been successfully used in a number of applications including choke coils,<sup>1-3,8-10</sup> mobile phones,<sup>2,3</sup> noise reduction devices,<sup>2,3</sup> computer hard disks,<sup>2,3</sup> and transformers.<sup>1-4,9,10</sup> Superior soft magnetic properties are attributed to the nanocrystalline  $\alpha''$ -(Fe, Si) phase (Fe<sub>3</sub>Si with D03 structure) in the size range of 10–15 nm diameter (radius 5–7.5 nm) and 70 % volume fraction.<sup>1,3-7,9-18</sup> Since its discovery, researchers have investigated FINEMET alloys to improve upon multiple soft magnetic properties by performing experiments followed by characterization using advanced diagnostic tools.<sup>3,5,6,9,11-13,16-18</sup>

In materials design, understanding the various processing-structure-property (PSP) linkages plays an important role in designing advanced materials. In particular, correlations between microstructure and desired properties,<sup>19-22</sup> are essential for the deployment

of new materials into service. In addition, composition variations and processing parameters (e.g., heat treatment schedule) play an integral role in modeling the microstructure(s) responsible for achieving desired properties, where optimizing processing parameters along with composition remains a challenging task.<sup>23</sup> As an alternative to costly experimentation, the CALPHAD approach allows for investigating the effect of composition variations and heat treatment on the size distribution and volume fraction of the phase(s) that are responsible for optimal or desired properties; indeed, it has been used for studying soft magnets containing amorphous phases<sup>24-26</sup> using the commercial software Thermocalc.<sup>27</sup> Recent studies indicate that simulations based on CALPHAD<sup>28,29</sup> are in need of efficiency improvements if they are to be used for optimization of the composition and heat treatment schedule. To address this challenge, it is important to develop models that can both replicate maximum information available from prior studies and, in addition, demonstrate effectiveness in optimizing the processing protocol. This effectiveness should not come, for example, from repeating the same calculations at different compositions, but rather from learning the results obtained in several selected cases in order to predict the behaviour at other compositions.

Machine learning approaches have been previous used

to help reduce the time required in the alloy design process.<sup>30–43</sup> Supervised machine learning approaches like artificial neural networks,<sup>41–45</sup>  $k$ -Nearest Neighbour algorithm ( $k$ -NN),<sup>42,43,46</sup> genetic programming,<sup>41–43,45,47</sup> kriging,<sup>48,49</sup> and unsupervised approaches such as Principal Component Analysis (PCA),<sup>32,33,37,39</sup> Hierarchical Clustering Analysis (HCA),<sup>31,33,37,38</sup> and Self Organizing Maps (SOM)<sup>30</sup> have been previously used in materials science and can also be helpful in this case. From an implementation point of view, there exist several open-source softwares to develop response surfaces or meta-models using several different concepts from artificial intelligence. A machine learning model based on results from the CALPHAD approach will serve as an important rapid screening tool before performing experiments and also in predicting outcomes in case of uncertainties in the composition of the material or in furnace temperature during annealing.

In this article, we present a combined CALPHAD-machine learning approach for optimizing composition along with processing parameters for FINEMET alloys by developing metamodels (response surfaces, or surrogate models) for the simulated crystallization of  $\text{Fe}_3\text{Si}$  domains. We have acquired data for mean radius and volume fraction of  $\text{Fe}_3\text{Si}$  nanocrystals through a recently developed precipitation model<sup>50</sup> in Thermocalc,<sup>27</sup> capable of simulating the nucleation and growth of  $\text{Fe}_3\text{Si}$  nanocrystals from an amorphous phase. Thereafter, we have used a  $k$ -Nearest Neighbour ( $k$ -NN) algorithm to generate computationally inexpensive metamodels to replace exhaustive Thermocalc modeling without any significant loss of accuracy. This way, we are able to demonstrate the efficacy of our combined CALPHAD-machine learning approach by predicting compositions and processing parameters that would lead to achieving the desired mean radius and volume fraction of  $\text{Fe}_3\text{Si}$  nanocrystals. The developed metamodels capture the established nucleation and growth evolution<sup>51,52</sup> within the CALPHAD approach, for the entire annealing timescale even for compositions and parameters that were not included in the training set for the metamodels. Another important observation is that the metamodels can predict outcomes in a fraction of the time taken by simulations in Thermocalc.<sup>53</sup> Last but not least, we propose Parallel Coordinates Charts (PCC)<sup>54</sup> for comprehensive visualization of the relationships between processing parameters and optimized quantities, and for rapid identification of the parameters that lead to crystallization of  $\text{Fe}_3\text{Si}$  nanocrystals in the desired size range and volume fraction. Our proposed approach helps reduce the alloy development time since it can serve as a tool for rapid screening of the multi-dimensional parameter space before performing experiments. As such, this combined machine learning and CALPHAD approach illustrates a case of addressing the challenge of simultaneously determining the effect of composition variation and processing parameters<sup>19–23</sup> on the microstructure and can be extended to other alloy systems.

## II. METHODS

Figure 1 shows the schematic flowchart of the process we followed in order to develop our combined CALPHAD-machine learning approach for optimization of nanocrystal size and volume fraction. This approach is enabled by a nucleation and growth model (precipitation model) in Thermocalc,<sup>55</sup> recently parameterized for FINEMET.<sup>50</sup> We used this model to generate data for mean radius and volume fraction of  $\text{Fe}_3\text{Si}$  nanocrystals grown upon annealing the amorphous material, data which serves as training set for developing metamodels. Analysis of the results created by the metamodels reveals correlations between the input parameters (composition, temperature, and time) and the optimized quantities. The three aspects (Figure 1) are described in some detail below.

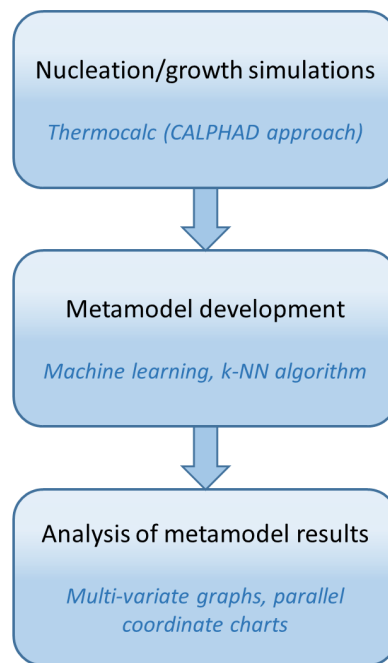


FIG. 1. Flowchart of steps followed in this work for a class of FINEMET alloy with composition  $\text{Fe}_{72.89}\text{Si}_{16.21}\text{B}_{6.9}\text{Nb}_3\text{Cu}_1$

### A. Generating data for developing a metamodel

To generate mean radius and volume fraction data, we have used the TC-PRISMA<sup>55</sup> module in Thermocalc, which relies on thermodynamic (TCFE8)<sup>53</sup> and mobility<sup>56</sup> databases. TC-PRISMA<sup>55</sup> uses the Kampmann-Wagner Numerical (KWN) method<sup>51,52</sup> for simulating nucleation and growth of precipitates during annealing. KWN is an extension of the Langer-Schwartz approach<sup>57</sup> and its modified form.<sup>58</sup> To use the precipitation model, several input quantities in TC-PRISMA<sup>55</sup> were previously parameterized<sup>50</sup> so that

the precipitation model simulates specifically and accurately the nucleation and growth of  $\text{Fe}_3\text{Si}$  nanocrystals during annealing. The FINEMET base composition is  $\text{Fe}_{82.35}\text{Si}_{9.21}\text{B}_{1.51}\text{Nb}_{5.64}\text{Cu}_{1.29}$  in weight %, or  $\text{Fe}_{72.89}\text{Si}_{16.21}\text{B}_{6.90}\text{Nb}_3\text{Cu}_1$  in atomic %; we will refer only to the latter in the reminder of the article. Simulations of precipitation were performed for new compositions  $\text{Fe}_{72.89+x}\text{Si}_{16.21-x}\text{B}_{6.90}\text{Nb}_3\text{Cu}_1$  generated by varying the content of Fe and Si by a quantity  $x$  ( $\leq x \leq 3$ ). Isothermal annealing was carried out at a set of temperatures between 490 °C and 550 °C in (increments of 10 °C) to for 2 hrs holding time. We obtained significant amounts of Thermocalc data for mean radius and volume fraction of  $\text{Fe}_3\text{Si}$  nanocrystals, which would serve as training set for machine learning stage of the workflow (Figure 1).

### B. $k$ -Nearest Neighbour Algorithm

The mean radius and volume fraction were generated in order to be used for creating response surfaces or meta-models to help in the design of future nanocrystalline FINEMET alloys. We use the  $k$ -NN algorithm<sup>46</sup> as implemented in the software modeFRONTIER<sup>59</sup> to construct the metamodels. This algorithm stores all the available information and predicts a new output (in this case, mean radius and volume fraction) based on a measure of similarity (distance function) of the new input with the stored cases. Specifically, to predict the new target/output that corresponds to a new input, the straightforward approach is to compute the average of the outputs of the first  $k$  nearest neighbors of the new input. In general, the average is weighted so that some neighbors contribute more to the average than others. In our work, we use  $k = 11$  neighbors for the metamodel describing the mean radius and volume fraction of  $\text{Fe}_3\text{Si}$  nanocrystals as functions of  $x$ , annealing temperature, and holding time.

### C. Parallel coordinates chart

Parallel Coordinates Chart (PCC)<sup>54,60</sup> is a powerful tool used for visualizing large and multivariate sets of data or results.<sup>54,60</sup> It has been successfully implemented in a number of applications such as visual and automatic data mining, optimization, process control, decision support, and approximations.<sup>54,60</sup> In PCC, a number of parallel (vertical) coordinate axes represent the  $n$  dimensions of a given set of data. Any particular data point in the  $n$ -dimensional space is represented by a line that connects single points on each of the  $n$  parallel coordinate axes.

We have five parallel coordinate axes in this work, three variable (input) axes,  $x$ , temperature, holding time, and two function (output) axes, mean radius and volume fraction. Significant amounts of data were created, i.e., 22,000 data sets generated from the precipitation model and 22,000 sets generated through the metamodel for

(new) randomly generated sets of variables ( $x$ , temperature, and time). In order to properly explore the variable space, we used the Sobol algorithm<sup>61</sup> for sampling the  $x$ , temperature, and time domains. We analyzed all data using PCC in order to find the parameters that should be followed (or avoided) so as to crystallize  $\text{Fe}_3\text{Si}$  nanocrystals in the desired range for mean radius (5-7.5 nm) and volume fraction ( $> 70\%$ ). Another reason was to explore the possibility of decreasing holding time during isothermal annealing without compromising on size range and volume fraction. This is the first instance of using PCCs in materials design.

## III. RESULTS AND DISCUSSION

### A. Analysis of training set results and of the metamodel

Using the data obtained from Thermocalc for few compositions and temperatures, we plot the mean radius and volume fraction as surface meshes in which one of the variables ( $x$ , temperature, or time) is fixed at a certain value, while the other two are allowed to vary over their respective ranges (Figures 2–6). In these mesh plots, surfaces appear stepped because they represent the training set in which  $x$  and temperature each vary in seven discrete, large steps. Even without a metamodel, these direct simulations show that one needs to avoid concentration deviations  $x$  larger than 0.5% since they would not lead to mean radius in the desired range (Figure 2).

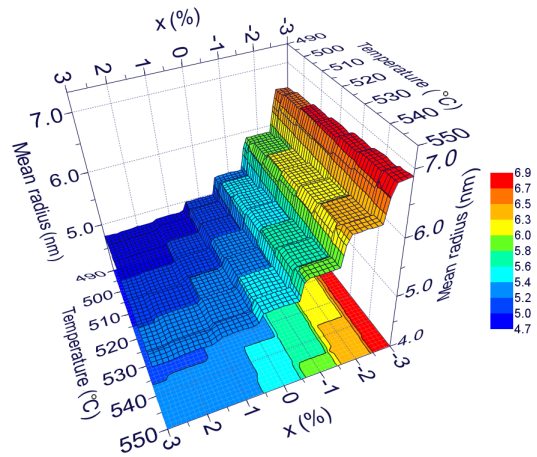


FIG. 2. Mean radius of  $\text{Fe}_3\text{Si}$  nanocrystals as a function of  $x$  and annealing temperature, for a holding time of 1 h.

Using the metamodels based on the  $k$ -NN algorithm trained on data in Figures 2–6, we develop the contour plots for mean radius and volume fraction as functions of temperature and  $x$ , for three annealing times (Figures 7, 8). In Figures 7 and 8, we show the 22,000 data sets that have not been used in the training of the kNN metamodel. Other ways to plot the results from the

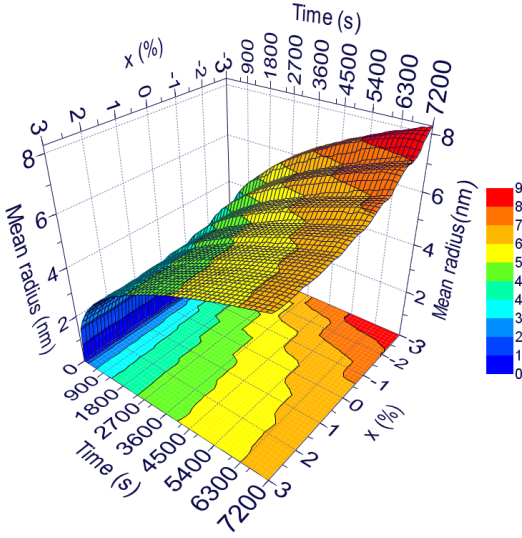


FIG. 3. Mean radius of  $\text{Fe}_3\text{Si}$  nanocrystals as a function of  $x$  and holding time, for a temperature of  $500^\circ\text{C}$ .

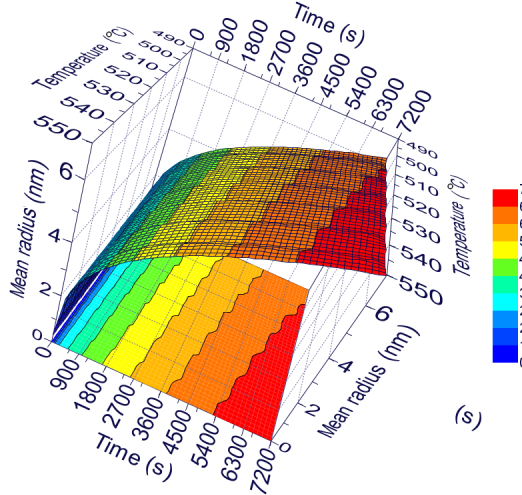


FIG. 4. Mean radius of  $\text{Fe}_3\text{Si}$  nanocrystals as a function of annealing temperature and holding time, for the nominal composition ( $x = 0$ ).

metamodels so as to aid the design process with three inputs ( $x$ , temperature, time) and two properties to optimize (radius and volume fraction) will be shown later.

Next, we focus on assessing the performance of the metamodels derived trained on the data in Figures 2–6).

### B. Testing the developed metamodel

To assess the usefulness of the metamodel for design, we compared its predictions for inputs that were not included in the training set, with Thermocalc results for the same new inputs. In order to sample the three-variable

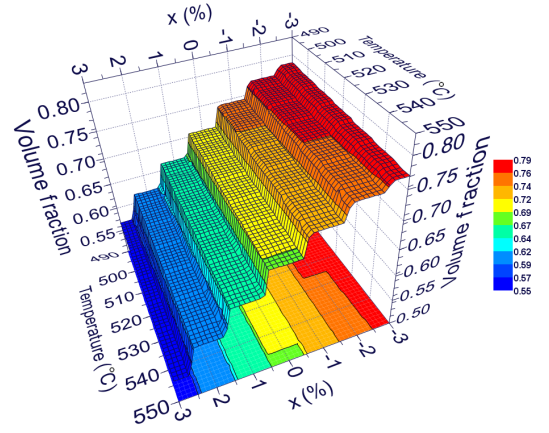


FIG. 5. Volume fraction of  $\text{Fe}_3\text{Si}$  nanocrystals as a function of annealing temperature and  $x$ , for 2 h holding time.

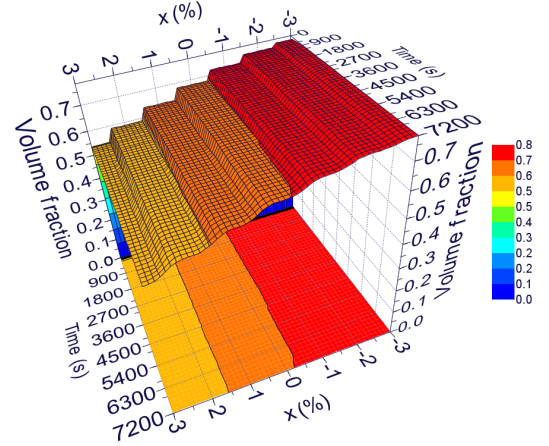


FIG. 6. Volume fraction of  $\text{Fe}_3\text{Si}$  nanocrystals as a function of holding time and  $x$ , at a temperature of  $550^\circ\text{C}$ .

space, we use Sobol sequences<sup>61</sup> to generate new random data points for the three processing parameters as follows: 140 points for  $x$  between  $-3\%$  and  $3\%$ , 12 points for temperatures between  $490$  and  $550^\circ\text{C}$ , and 12 points for annealing time up to 2 h.

To illustrate comparisons between the metamodel predictions and direct Thermocalc results, we selected three pairs of processing parameters, ( $x = 0.75, 515^\circ\text{C}$ ), ( $x = 0, 515^\circ\text{C}$ ) and ( $x = -2.95, 545^\circ\text{C}$ ). Figure 9 and 10 show both the metamodel predictions (lines) and the Thermocalc calculations (dots) for the mean radius of  $\text{Fe}_3\text{Si}$  nanocrystals and their volume fraction, respectively. As apparent from these figures, there are only small deviations of the predictions of the metamodel from the direct Thermocalc results for the entire annealing duration considered. Referring to the 3D surface plots (Figures 2–6), we explained that their stepped appearance was due to the sparseness of the training sets for temperature and composition deviation  $x$ . Despite the sparseness of the training data, we note that the developed response



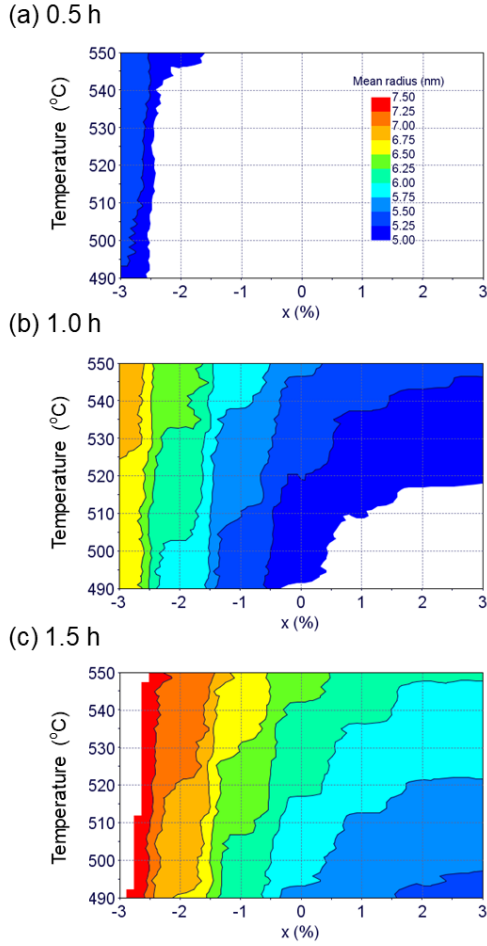


FIG. 7. Mean radius predicted from the metamodel after (a) 0.5 h, (b) 1.0 h, and (c) 1.5 h annealing time. Only the desired values (5 – 7.5 nm) are shown in the contour plots.

surfaces (metamodels) are able to capture closely the trends observed during nucleation and growth of  $\text{Fe}_3\text{Si}$  nanocrystals for both mean radius (Figure 9) and volume fraction (Figure 10), even though the machine learning algorithm was not exposed to the physical principles of nucleation and growth: this illustrates the predictive power of the machine learning approach in this case. We have tested many other sets of input parameter sets as well and have concluded that the metamodel developed via the  $k$ -Nearest Neighbour algorithm is sufficiently robust that its predictions can be verified back and forth for random compositions and processing parameters.

To better emphasize its use for design purposes, we have estimated the time taken by the metamodel to drive experimental predictions for different processing parameters. Table I shows a comparison of time estimates for experiments (annealing estimated at 1 h per sample at a given temperature), direct CALPHAD calculations, and the metamodel: as seen in the table, for very large datasets (44,000 datasets in Table I) the time decreases from years (experiments) to minutes (meta-

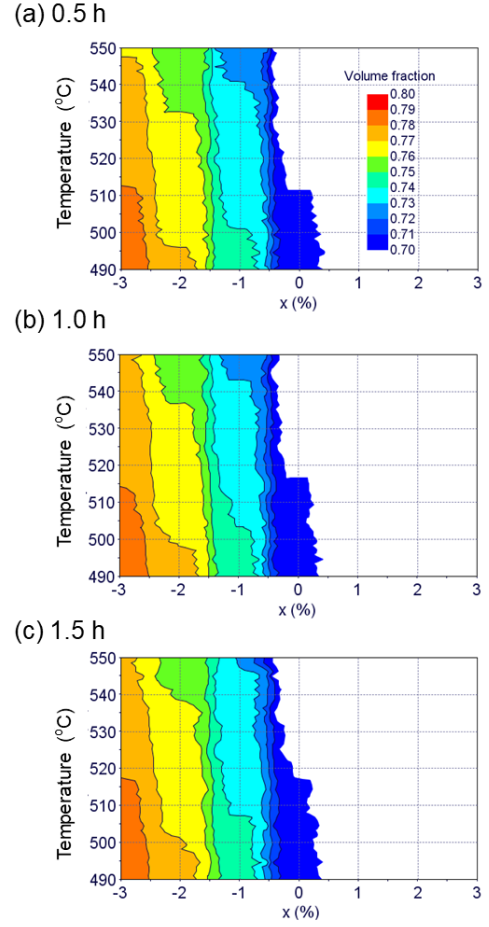


FIG. 8. Volume fraction of the nanocrystalline phase predicted from the metamodel after (a) 0.5 h, (b) 1.0 h, and (c) 1.5 h annealing time. Only the desired values ( $\geq 0.7$ ) are shown in the contour plots.

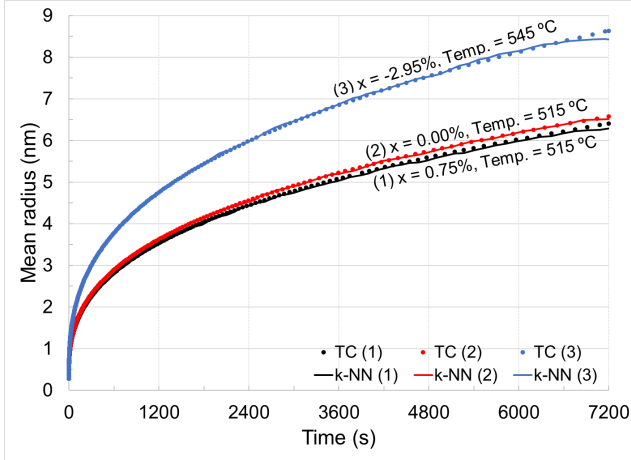
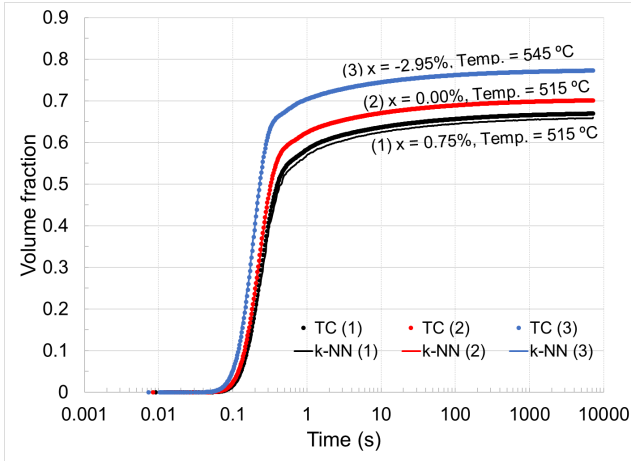
model). In practice, the experiments simply would not be performed for this many datasets and researchers would necessarily have to make inferences from much fewer sets of data. The availability of a metamodel in this case allows for the rapid identification of experimental conditions/parameters that lead to optimal mean radius and volume fraction.

### C. Other representations of the metamodel results for use in multivariate design space

We note that contour plots such as those in Figures 7 and 8 do not fully show all of the information that practitioners may need. In particular, creating multiple time slices could make the use of the metamodels cumbersome. To further pursue the idea of charting the parameter space, we are pursuing graphical ways to represent all the correlations between the optimized quantities and the input parameters; in other words, we develop graphical ways to show the predictions of the metamodel so

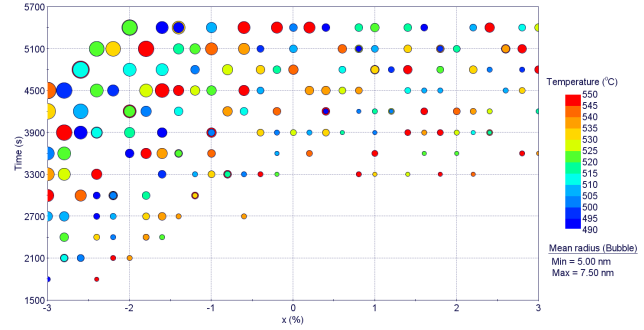
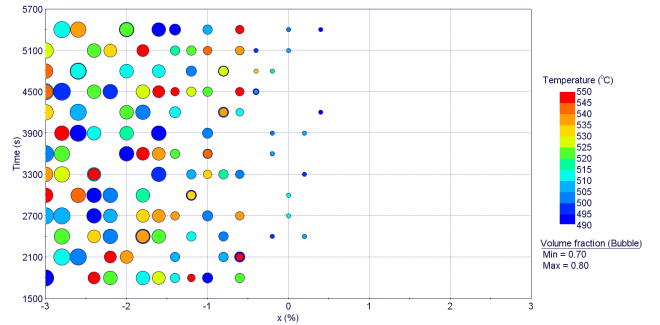
TABLE I. Comparison of time estimates between experiments, CALPHAD, and machine learning approach.

Set of parameters	Average Annealing time		
	Experiments	CALPHAD (Thermocalc)	Machine Learning
1	1 hour	30 Seconds	Developing metamodel: Less than 2 Minutes
44,000	44,000 Hours = 1,833 Days = <b>5 Years (Just annealing)</b>	366 Hours = <b>15.28 Days</b>	Less than 2 minutes <b>Total: Less than 4 minutes.</b>

FIG. 9. Mean radius ( $\text{Fe}_3\text{Si}$ ) vs. Time: Comparison between Thermocalc (TC) and metamodel (KN) prediction.FIG. 10. Volume fraction( $\text{Fe}_3\text{Si}$ ) vs. Time: Comparison between Thermocalc (TC) and metamodel (KN) prediction.

as to facilitate their use for design purposes. One such way is to represent each optimized quantity (mean radius and volume fraction) in terms of all of the three inputs using “bubble” plots (Figures 11 and 12), in which the inputs are on the horizontal axis ( $x$ ), vertical axis (time), and on a color scale (temperature). For such representations, the mean radius or the volume fraction predicted by the metamodel are shown as circles of different radii

(Figures 11, 12). Armed with an interactive plot (such as, for example, those created in modeFRONTIER), a practitioner seeking to design FINEMET alloys would choose a mean radius, and then simply read out from the bubble plots (Figure 11) various possibilities (i.e.,  $x$ , temperature, and time) leading to that mean radius. The value added by such plots is that they can supply multiple combinations of parameters for the same mean radius or volume fraction, thereby providing choices for experimentalists. For example, it can be beneficial to choose lower temperatures and shorter annealing times, and which would be enabled by minor composition variations.

FIG. 11. Mean radius (circles) for different values of  $x$ , annealing time, and temperature. For clarity, only a subset of 300 data sets is shown.FIG. 12. Volume fraction for different values of  $x$ , annealing time, and temperature. To avoid overlaps, only a subset of 300 data sets is shown.

While such bubble plots show each optimized quantity

for all the three inputs, one can encounter optimization problems with more than three inputs and more than two optimized quantities. We propose that, in general, all inputs and outputs can be shown on parallel coordinates, as mentioned in the Methods section. PCCs<sup>54</sup> are an effective way to demonstrate the relationships between desired properties (output) and the input parameters for high dimensional data, in which the inputs and outputs stand on equal footing: any input or output quantity is shown on one of the parallel axes. We can use PCCs to assess the effect of each separate input on the design quantities (Figure 13), or we can choose design targets (e.g. mean radius set a desired values) and then select input parameters from the many sets that lead to that design target (Figures 14, 15).

Figures 13(a),(b), and (c) show the effect of  $x$ , temperature, and time, respectively on the mean radius and volume fractions. The same 44,000 data sets were plotted in the three panels of Figure 13, with difference that the color scale from red to blue is placed on the different input axes for ease of separating the individual effects on mean radius and volume fraction. Consistent with the other analysis (Figure 7), lowering the concentration deviation  $x$  (Figure 13(a)) increases the mean radius and the volume fraction. The effect of temperature is not so obvious from these PCCs with large amounts of data, since it is strongly coupled with the effect of annealing time. As such, all temperatures can lead to the desired range of mean radius and volume fraction, provided that the annealing time is greater than 0.5 h (Figures 13(b,c)). In practice, the PCC charts are interactive: a user can simply click select a line crossing the axis of a quantity to be optimized, and then the values for all the parallel coordinates are displayed: in particular, a large set of input triplets. For clarity, we illustrate this point here with a very small amount of (selected) data. For clarity, in Figure 14 we display only three such sets of input triplets corresponding to a selected mean radius of 6 nm. In this figure, the nominal composition requires 550 °C and annealing for 1.28 h (4600 s). Allowing the concentration to deviate from the nominal one ( $x = -1.45\%$ ,  $-2.25\%$ ) can lead to lowering both the temperature and the annealing duration (Figure 14). This is precisely the value that the metamodel brings to the design process, i.e. providing accurate, rapidly computed input parameters that guide the processing so as to obtain desired outputs (mean radius and volume fraction) while often allowing for time and cost optimizations as well. For completeness, we also present the PCCs with separate color scales for the two

optimized properties (Figure 15).

#### IV. CONCLUSIONS

From the results of the metamodel, there are several general conclusions pertaining the effects of input parameters on mean radius and volume fraction. For short anneal times (0.5 h, Figure 7(a)), mean radius in the desired range can be achieved for any temperature provided that  $x < -2.5\%$ . When annealing is sufficiently long (2 h), then all compositions  $x$  investigated can lead to mean radius in the desired range (7(c)). A volume fraction  $> 0.7$  can be achieved at all temperatures in the range and all times longer than 0.5 h, provided the composition below a threshold,  $x < 0.5\%$  (Figures 8, 12).

The metamodels provide not only general trends, but, more importantly, specific and multiple inputs that lead to the desired output (mean volume and volume fraction). These are important choices for design, which can be carried out based completely based on the metamodel simulation results. The PCCs (Figures 13 and 15), in particular, would help practitioners decide the inputs based on their material composition ( $x$ ) and perhaps even economic considerations (lower anneal temperature and/or time for large scale production).

The present results illustrate a robust approach for discovering relationships between processing and alloy structure/morphology in nanocrystalline alloys. Taking a perspective view on these results, the combined CALPHAD-machine learning approach can be in principle generalized for many other design situations in which structure or morphology optimization via processing conditions is necessary. Key factors for obtaining predictive metamodels would be to ensure all important inputs are considered, and to judiciously select the machine learning technique based on with the characteristics of the training data available.

#### V. ACKNOWLEDGMENTS

The authors acknowledge the financial support from the National Science Foundation through Grant. No. DMREF-1629026.

#### VI. REFERENCES

---

\* Corresponding Authors:

† rajeshjha@mines.edu

‡ cciobanu@mines.edu

<sup>1</sup> Y. Yoshizawa, S. Oguma, and K. Yamauchi, *Journal of Applied Physics* **64**, 6044 (1988).

<sup>2</sup> Hitachi, “Finemet,” (2017).

<sup>3</sup> M. A. Willard and M. Daniil, *Handbook of Magnetic Materials* **21**, 173 (2013).

<sup>4</sup> G. Herzer (Elsevier, 1997) pp. 415 – 462.

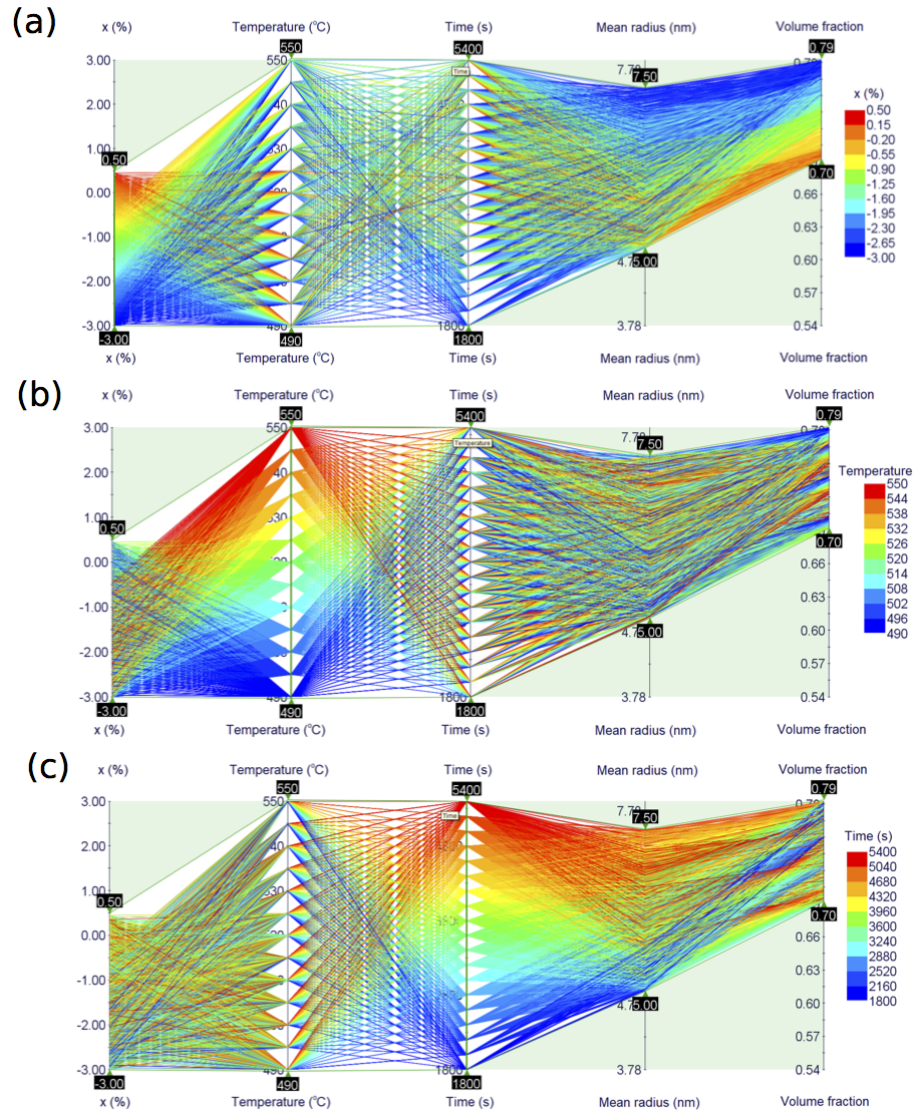


FIG. 13. Parallel coordinates chart for input variables (a)  $x$ , (b) temperature, and (c) time from 44,000 sets of data.

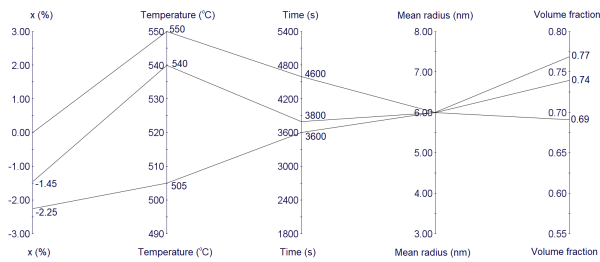


FIG. 14. Parallel coordinates chart for mean radius of  $\text{Fe}_3\text{Si}$  nanocrystals. For clarity, this PCC shows only three of the ( $x$ , temperature, time) sets that lead to one desired mean radius (6 nm).

- <sup>6</sup> H. Lashgari, D. Chu, S. Xie, H. Sun, M. Ferry, and S. Li, *Journal of Non-Crystalline Solids* **391**, 61 (2014).
- <sup>7</sup> N. Mattern, A. Danzig, and M. Müller, *Materials Science and Engineering: A* **194**, 77 (1995).
- <sup>8</sup> M. E. McHenry, M. A. Willard, and D. E. Laughlin, *Progress in Materials Science* **44**, 291 (1999).
- <sup>9</sup> G. Herzer, *Physica Scripta* **1993**, 307 (1993).
- <sup>10</sup> G. Herzer, *Acta Materialia* **61**, 718 (2013).
- <sup>11</sup> J. Ayers, V. Harris, J. Sprague, W. Elam, and H. Jones, *Nanostructured Materials* **9**, 391 (1997).
- <sup>12</sup> F. van Bouwelen, J. Sietsma, and A. Van Den Beukel, *Journal of non-crystalline solids* **156**, 567 (1993).
- <sup>13</sup> G. Herzer, *Materials Science and Engineering: A* **133**, 1 (1991).
- <sup>14</sup> G. Herzer, S. Flohrer, and C. Polak, *IEEE Transactions on Magnetics* **46**, 341 (2010).
- <sup>15</sup> G. Herzer, *Handbook of magnetism and advanced magnetic materials* (2007).

<sup>5</sup> K. Hono, A. Inoue, and T. Sakurai, *Applied physics letters* **58**, 2180 (1991).



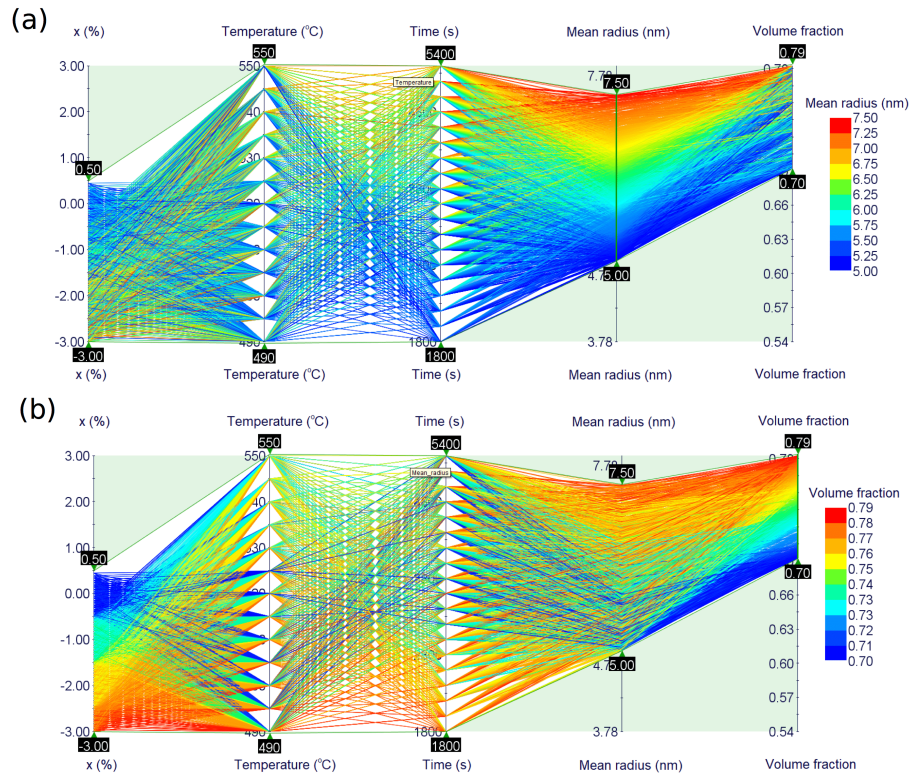


FIG. 15. Parallel coordinates charts obtained from 44,000 sets of data for (a) mean radius and (b) volume fraction (separate color legends) of Fe<sub>3</sub>Si nanocrystals.

- <sup>16</sup> M. T. Clavaguera-Mora, N. Clavaguera, D. Crespo, and T. Pradell, *Progress in Materials Science* **47**, 559 (2002).
- <sup>17</sup> C. Conde and A. Conde, *Materials Letters* **21**, 409 (1994).
- <sup>18</sup> K. Hono, D. Ping, M. Ohnuma, and H. Onodera, *Acta materialia* **47**, 997 (1999).
- <sup>19</sup> A. Khosravani, A. Cecen, and S. R. Kalidindi, *Acta Materialia* **123**, 55 (2017).
- <sup>20</sup> E. Popova, T. M. Rodgers, X. Gong, A. Cecen, J. D. Madison, and S. R. Kalidindi, *Integrating Materials and Manufacturing Innovation* **6**, 54 (2017).
- <sup>21</sup> N. H. Paulson, M. W. Priddy, D. L. McDowell, and S. R. Kalidindi, *Acta Materialia* **129**, 428 (2017).
- <sup>22</sup> E. A. Pfeif and K. Kroenlein, *APL Materials* **4**, 053203 (2016), <http://aip.scitation.org/doi/pdf/10.1063/1.4942634>.
- <sup>23</sup> A. Agrawal, P. D. Deshpande, A. Cecen, G. P. Basavarsu, A. N. Choudhary, and S. R. Kalidindi, *Integrating Materials and Manufacturing Innovation* **3**, 8 (2014).
- <sup>24</sup> A. Takeuchi and A. Makino, *Materials Transactions* **55**, 1852 (2014).
- <sup>25</sup> A. Takeuchi, Y. Zhang, K. Takenaka, and A. Makino, *Journal of Applied Physics* **117**, 17B737 (2015).
- <sup>26</sup> T. Takahashi, K. Yoshida, Y. Shimizu, A. Setyawan, M. Bito, M. Abe, and A. Makino, *AIP Advances* **7**, 056111 (2017).
- <sup>27</sup> THERMOCALC, "Website," (2017).
- <sup>28</sup> H. Larsson and L. Höglund, *Calphad* **50**, 1 (2015).
- <sup>29</sup> R. Pillai, T. Galiullin, A. Chyrkin, and W. Quadakkers, *Calphad* **53**, 62 (2016).
- <sup>30</sup> R. Jha, G. S. Dulikravich, N. Chakraborti, M. Fan, J. Schwartz, C. C. Koch, M. J. Colaco, C. Poloni, and I. N. Egorov, *Materials and Manufacturing Processes* **32**, 1067 (2017).
- <sup>31</sup> R. Jha, G. Dulikravich, M. Colaco, M. Fan, J. Schwartz, and C. Koch, in *Properties and Characterization of Modern Materials*, Vol. 33 (Springer Singapore, 2017) pp. 261–284.
- <sup>32</sup> R. Jha, G. S. Dulikravich, N. Chakraborti, M. Fan, J. Schwartz, C. C. Koch, M. J. Colaco, C. Poloni, and I. N. Egorov, *Journal of Alloys and Compounds* **682**, 454 (2016).
- <sup>33</sup> R. Jha, FIU Electronic Theses and Dissertations. 2621 (2016).
- <sup>34</sup> M. Fan, Y. Liu, R. Jha, G. S. Dulikravich, J. Schwartz, and C. Koch, *IEEE Transactions on Magnetics* **52**, 1 (2016).
- <sup>35</sup> M. Fan, Y. Liu, R. Jha, G. S. Dulikravich, J. Schwartz, and C. Koch, in *13th Joint MMM-Intermag Conference*, , San Diego, California. (2016).
- <sup>36</sup> R. Jha, G. S. Dulikravich, and M. J. Colaco, in *23rd ABCM International Congress of Mechanical Engineering - COBEM 2015, December 6-11 (2015), Rio de Janeiro, Brazil*. (ABCM International Congress of Mechanical Engineering, 2015).
- <sup>37</sup> R. Jha, G. S. Dulikravich, M. J. Colaco, I. N. Egorov, C. Poloni, N. Chakraborti, M. Fan, J. Schwartz, and C. C. Koch, in *MSE/T 2015, Columbus, OH. (MST 2015, October 4-8 (2015), Columbus, OH., 2015)*.
- <sup>38</sup> R. Jha, G. S. Dulikravich, M. J. Colaco, M. Fan, J. Schwartz, and C. C. Koch, in *ACE-X2015, June 29th*

- July 2nd (2015), Munich, Germany. (ACE-X2015, June 29th - July 2nd (2015), Munich, Germany., 2015).
- <sup>39</sup> R. Jha, G. Dulikravich, N. Chakraborti, M. Fan, J. Schwartz, C. Koch, and M. Colaco, in *Proc. ICMM4* (2015) pp. 1–19.
  - <sup>40</sup> M. Fan, Y. Liu, R. Jha, G. S. Dulikravich, J. Schwartz, and C. Koch, *Journal of Magnetism and Magnetic Materials* **420**, 296 (2016).
  - <sup>41</sup> R. Jha, F. Pettersson, G. Dulikravich, H. Saxen, and N. Chakraborti, *Materials and Manufacturing Processes* **30**, 488 (2015).
  - <sup>42</sup> R. Jha, G. S. Dulikravich, M. Fan, J. Schwartz, C. Koch, and C. Poloni, in *CONEM2014, At Uberlandia, Brazil* (2014).
  - <sup>43</sup> R. Jha, G. S. Dulikravich, F. Pettersson, H. Saxen, and N. Chakraborti, in *ASME Symposium on Elevated Temperature Application of Materials for Fossil, Nuclear, and Petrochemical Industries* (2014).
  - <sup>44</sup> F. Pettersson, N. Chakraborti, and H. Saxén, *Applied Soft Computing* **7**, 387 (2007).
  - <sup>45</sup> R. Jha, P. K. Sen, and N. Chakraborti, *steel research international* , 219 (2014).
  - <sup>46</sup> K.-N. N. Algorithm, “K-nn,” (2017).
  - <sup>47</sup> B. K. Giri, F. Pettersson, H. Saxén, and N. Chakraborti, *Materials and Manufacturing Processes* **28**, 776 (2013).
  - <sup>48</sup> P. D. Pantula, S. S. Miriyala, and K. Mitra, *Materials and Manufacturing Processes* **32**, 1162 (2017).
  - <sup>49</sup> T. Chugh, N. Chakraborti, K. Sindhya, and Y. Jin, *Materials and Manufacturing Processes* **32**, 1172 (2017).
  - <sup>50</sup> R. Jha, D. Diercks, A. Stebner, and C. V. Ciobanu, arXiv:1709.08306 [cond-mat.mtrl-sci] (2017).
  - <sup>51</sup> R. Kampmann and R. Wagner, in *Proc. 2nd Acta-Scripta Metall. Conf., Pergamon, Oxford* (1984) pp. 91–103.
  - <sup>52</sup> R. Wagner, R. Kampmann, and P. W. Voorhees, *Materials science and technology* (1991).
  - <sup>53</sup> THERMOCALC, “Tcfe8 database,” (2017).
  - <sup>54</sup> A. Inselberg, “Introduction,” in *Parallel Coordinates: Visual Multidimensional Geometry and Its Applications* (Springer New York, New York, NY, 2009) pp. 1–5.
  - <sup>55</sup> THERMOCALC, “Tcprisma,” (2017).
  - <sup>56</sup> THERMOCALC, “Tcfe8, mobfe3 database,” (2017).
  - <sup>57</sup> J. Langer and K. Schwartz, *Physical Review A* **21**, 948 (1980).
  - <sup>58</sup> Computherm, “Precipitation simulation,” (2017).
  - <sup>59</sup> “Website,” (2017).
  - <sup>60</sup> A. Inselberg, “Parrellel coordinates chart algorithm,” (2017).
  - <sup>61</sup> I. Sobol’, *USSR Computational Mathematics and Mathematical Physics* **7**, 86 (1967).